PAPER • **OPEN ACCESS**

Anisotropic deformation of colloidal particles under 4 MeV Cu ions irradiation

To cite this article: E A Dawi *et al* 2022 *Mater. Res. Express* **9** 086506

Materials Research Express

PAPER

Anisotropic deformation of colloidal particles under 4 MeV Cu ions irradiation

E A Dawi[1], E Mustafa[2] and T Siahaan[3]

[1] Nonlinear Dynamics Research Centre (NDRC), Ajman University, PO Box 346, United Arab Emirates
[2] Department of Science and Technology (ITN), Linköping University, Campus Norrköping, 60174 Norrköping, Sweden
[3] Department of Applied Physics, Eindhoven University of Technology, 5600 MB Eindhoven, The Netherlands

E-mail: e.dawi@ajman.ac.ae

Keywords: silica dispersion, stöber method, silica- au core-shell, au colloids, anisotropic deformation, localized surface plasmons

OPEN ACCESS

RECEIVED
20 June 2022

REVISED
3 August 2022

ACCEPTED FOR PUBLICATION
8 August 2022

PUBLISHED
19 August 2022

Abstract

Anisotropic deformation of colloidal particles was investigated under ion irradiation with 4 MeV Cu ions. In this study, 0.5 μm-diameter colloidal silica particles, 0.5 μm-diameter Au-silica core–shell particles, and 15 nm-diameter Au colloids embedding in a planar Si/SiO_2 matrix were irradiated with 4 MeV Cu ions at room temperature and normal incidence. In colloidal silica particles, ion beam irradiation causes dramatic anisotropic deformation; silica expands perpendicular to the beam and contracts parallel, whereas Au cores elongate. Au colloids in a planar SiO_2 matrix were anisotropically transformed from spherical colloids to elongated nanorods by irradiating them with 4 MeV Cu ions. The degree of anisotropy varied with ion flux. Upon irradiating the embedded Au colloids, dark-field light scattering experiments revealed a distinct color shift to yellow, which indicates a shift in surface plasmon resonance. A surface plasmon resonance measurement reveals the plasmon resonance bands are split along the arrays of Au colloids. Our measurements have revealed resonance shifts that extend into the near-infrared spectrum by as much as 50 nm.

Introduction

Noncrystalline objects are anisotropically deformed by swift heavy ions, and it has been demonstrated that the ion tracks relax at temperatures higher than flow temperatures T^* [1–4]. Anisotropic deformation observed at macroscale is likely caused by accumulated ion effects. Amorphous materials are rapidly heated by ion beams with MeV energy passing through them. At low temperatures, anisotropic strain results in a rapid cooling rate (10^{12} K s^{-1}) of the track. Quantitatively describing the deformation observed can be accomplished using a continuum mechanics model incorporating the deposited ion energy, the material's thermal and mechanical properties, and particle-substrate interaction size effects. A cylindrical shape is always predicted, namely a shortening of irradiated materials along the ion direction and a simultaneous extension perpendicular to it. A key element of the prediction is both the anisotropy of the ion track and the thermal expansion of the material within the track, combined with the relaxation of the shear stress across T^*. To date, anisotropic plastic deformation has been extensively studied in two-particle systems; both dielectric colloidal silica and metal particles embedded in dielectric films. Changing the irradiation conditions can change the shape and morphology of colloidal silica particles and embedded metal particles. Particles with this property are useful for applications in nanophotonics [5, 6], improved LEDs [7], improved solar cells [8, 9], chemical (bio)sensors [10], and medical treatment and diagnostics [11]. Aspects such as attenuation factors and field enhancement factors (in gold) become more prominent as spherical shapes are changed to nanorods and nanowires. As described by D'Orléans *et al* [12–14], cobalt nanoparticles (Co NPs) embedded in silica were rapidly exposed to heavy ion beams in order to modify their shape. The size and shape of particles change as a result. A number of studies have examined in detail how ion beams induce metal nanoparticles to deform, and they all resulted in nanorods or nanowires that were aligned along the ion beam direction [15–25]. A system consisting of a core of Au and a shell of silica was investigated by Polman's group [26–28]. Ion-induced shape deformation has also been interpreted

using the thermal spike model [29–34]. It has been demonstrated that different morphologies can be obtained based on the size of the initial sample by researchers at CNRS in Caen, France [35]. Precision aligned nanorods can be easily fabricated using swift heavy ion beam irradiation [36–44]. An investigation by the author and co-workers [45] examined the relationship between metal particle size and deposited energy. Their findings showed that the shape changes usually occur in the energy range when heavy ions are most susceptible to stopping electronically. Nevertheless, only a few experiments have been conducted to figure out how much ion energy is required to deform micro- and nano-objects. On the basis of high-energy deformation measurements of microscopic dielectric silica colloids, it cannot be expected that ion beams will deform dielectric silica particles below 0.6 keV n m^{-}. In a comparative analysis of experiments with different ion energies, it was found that colloidal metal particles deform only above a threshold of 3.3 keV nm^{-1} loss in silica [28]. Based on extensive experiments on colloidal metal particles embedded in silica films, the author and colleagues demonstrate a size-dependent electronic stopping threshold of 3–4 keV nm^{-1} below which, they remain spherical under heavy ion bombardment [46]. Using micro and nano-colloid arrays and single particles, we aim to extend the susceptibility of micro- and nano-colloids to deformation near electronic energy losses below 2 keV nm^{-1} in silica. Among the particles investigated are colloidal silica particles, colloidal Au-silica core–shell particles with a diameter of 0.5 μm (with a relative polydispersity of 3%), and colloidal Au particles embedded in planar Si/SiO_2 films. Each sample was irradiated with 4 MeV Cu^{+2} ions at RT and normal incidence with a fluence of about a few 10^{14} ions cm^{-2}. We present here a significant advance over previous work in that we combine two separate particle systems, namely colloidal Au and silica particles, that have been studied and discussed separately in the literature.

Materials and methods

As received, the following chemicals and materials were used to prepare the samples: Tetraethoxysilane (TEOS, Merck), ethanol/methanol (Merck), ammonia solution (Merck), chloric acid (60%, Merck), 3-aminopropyl (trimethoxy) silane (APTEMS, Sigma-Aldrich 98%), and hydroxylamine hydrochloride solution (25%, Aldrich). In the experiment, University-wafer provided N-type Si substrates (100) with a resistivity of 1–10 Ω.cm and thermally grown silicon oxide (SiO_2) of about 200 nm. British Bio-cell International (BBI) provided charge-stabilized colloidal Au particles with a diameter of 15 nm (±3 nm) for use in the present study. Demineralized and distilled water were used. Silica particles were prepared by hydrolysis and condensation polymerization of tetraethoxysilane (TEOS) in ethanol, water, and ammonia mixture by the Stöber method [47, 48]. Using detergent, demineralized water, and extensive rinsing and drying, all glassware used in the Stöber synthesis was properly cleaned. We rapidly added distilled TEOS (75 ml) to a mixture of distilled ethanol and ammonia (25%), while vigorously stirring. After a few minutes, the mixture developed whitish turbidity due to the build-up of silica particles. We synthesized monodisperse silica colloids with a diameter of about 500 nm and a thickness of 40 nm. A core–shell colloidal structure of silica and gold was prepared by functionalizing the gold particles with polyvinylpyrrolidone [28, 49]. A Stöber growth of the silica shell was then induced by transferring the colloids to ethanol. We dried a droplet of the colloidal suspensions on a Si(100) substrate. This was then purified in a 1.0 M KOH-ethanol solution under nitrogen flow for 10 min and evaporated to leave the typical surface coverage well below the monolayer. A Si_3N_4 membrane embedded in a Si wafer was used for TEM analysis of the colloids. A planar silica film containing monodisperse metallic Au colloids was prepared by rinsing Si/SiO_2 samples with 99.9% ethanol, immersing them in distilled water for a few minutes, and then drying them with nitrogen. The native oxide layer has a thickness of about 200 nm. To ionize the substrates, 25 ml ethanol was mixed with 4.5 ml 2-Aminopropyltriethoxy/methylsilane (APTEMS) (Sigma-Aldrich 98.5%) about 0.94 g ml^{-1}. We allowed the substrates to react for 1.5–2 h. A stream of air was used to dry the substrates after they had been washed with highly purified methanol (99%) and distilled water. The surface was applied with a 15 nm diameter droplet of charge-stabilized monodisperse Au colloids. It is assumed the Si/SiO_2 surface will acquire an induced positive surface charge, allowing the negatively charged citrate groups on the colloidal Au surface to couple with each other. On top of the Si/SiO_2-Au NPs structure, a layer of silicon dioxide with a thickness of 150–200 nm was sputtered reactively, confining the Au colloids this way within about 350–400 nm thick silica sandwich. Several publications describe the deposition method for colloidal metal particles, such as [50, 51]. In this study, the size and shape of colloidal silica and gold particles were measured using scanning electron microscopy (SEM) observed under a 200 keV electron beam, atomic force microscope (AFM) in tapping mode, and cross-sectional transmission electron microscopy (TEM). Images from SEM show that the silica colloids, including the Au–silica core–shell colloids, measure about 0.5 μm in diameter (with a polydispersity of 3%). From the height profiles of the AFM images and high-resolution X-TEM analysis, we determined that the Au colloidal particles embedded in the Si/SiO_2 films before irradiation were about 15 nm in diameter with a deviation of about ±2 nm.

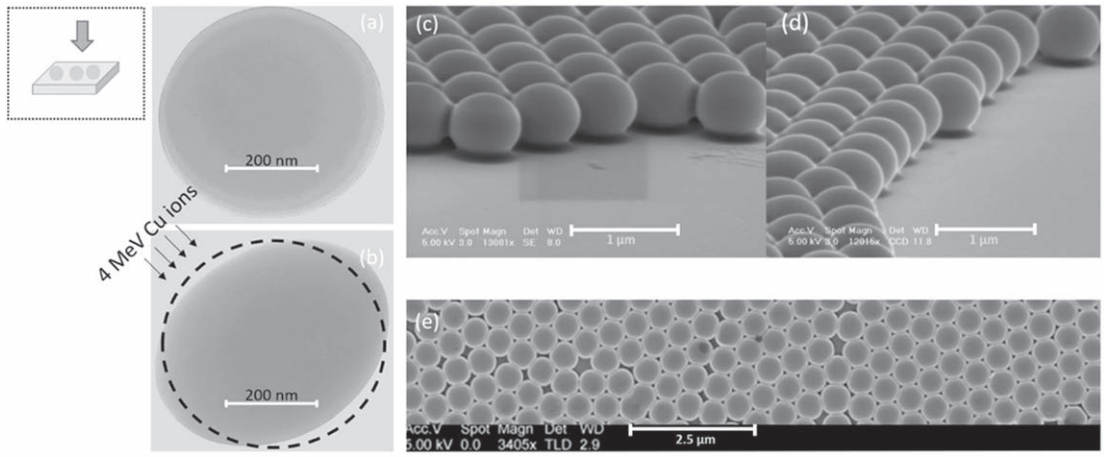

Figure 1. Transmission electron microscopy (TEM) images of colloidal silica particles with a diameter of 0.5 μm before and after irradiation with 4 MeV Cu ions, (a) and (b), respectively. Side-view scanning electron microscopy images (SEM) of the silica colloids, (c), and (d), respectively, and top-view of the silica colloids taken perpendicular to the plane of the colloids (e). The inset shows the configuration of the samples and the direction of the ion beam.

In order to ensure an ultimate contact between the Au colloids and surrounding SiO_2, the Si/SiO_2-Au colloids samples (total of 350–400 nm thickness) were annealed in an open furnace at 910 °C for approximately 25 min before irradiation. Irradiations were performed with a beam of 4 MeV Cu^{+2} ions, corresponding to an electronic stopping of 1.9 keV nm^{-1} in silica with a fluence of a few 10^{14} ions cm^{-2} RT and normal incidence geometry. By electrostatically sweeping the beam, homogeneous irradiation was obtained through an aperture of 2×2 cm^2. Irradiation fluence is calculated by multiplying the ion current density by the irradiation time. To improve the thermal contact between the cooled substrate holder and the sample, vacuum grease was used on the backside of the sample. It should be noted that the actual temperature of the colloid may be higher than the temperature of the holder during irradiation. Calculations of the ion range and the electronic energy loss of the 4 MeV Cu ions were made using the SRIM 2008 code [52]. The ion range has been verified as being far larger than the diameter and thickness of the colloidal silica films. Rutherford backscattering spectrometry (RBS) has been used to determine the relative change of Au peak width in response to the deformation of Au colloids embedded in Si/SiO_2 films. In addition to being able to retrieve the backscattering cross-section of each element, RBS allows the analysis of compositional thin films less than 1 μm thick. An RBS analysis involves directing a high-energy (2 MeV He^{2+}) beam of light ions onto a sample and observing the energy distribution and yield of the backscattered He^{2+} ions at a given angle. As such, RBS measurements have been used for obtaining quantitative compositional depth profiles from the elements contained in the sample without contributing to its deformation. An optical microscope that uses a dark-field scattering technique was used to examine the ion shaping effects in Au colloids embedded in Si/SiO_2 after irradiation, which exploits the phenomenon where the surface plasmon resonance of metal colloids can be redshifted by changing their size aspect ratio.

Results and discussion

Using 4 MeV Cu ions applied at RT and normal incidence, we studied the shape changes induced by ion-induced irradiation of a variety of colloidal particles, including silica particles (0.5 m diameter), Au-silica core–shell particles (15 nm core–0.5 m shell), and embedded colloidal Au particles (15 nm diameter) with an electronic energy loss of 2 keV nm^{-1}. Figure 1 shows TEM images of silica particles before and after irradiation (a) and (b), respectively on the Si wafer on which the silica colloids were synthesized. As an inset of figure 1, one can see the configuration of the colloidal particles under irradiation. A set of black arrows tilted at 45° degrees from the sample surface indicate the direction of the ion beam. As shown in figure 1(a), the synthesized silica colloids are spherical, with a diameter of about 0.5 μm. Figure 1(b) shows that the colloidal silica particle expands as it is exposed to 4 MeV Cu ions with a fluence of 8.5×10^{14} ions cm^{-2} and contracts parallel to the direction of the ion beam. A dashed line is drawn in figure 1(b) to represent the circumference of the original colloid. Calculations indicate that the deformed silica particle has a transverse diameter of ~650 nm, an increase of about 30%. This represents a decrease of about 20% in longitudinal diameter (along the ion beam direction). Shape anisotropies are observed with a size aspect ratio (major to minor axis) of 1.6. Based on a simple calculation that takes into account a relative polydispersity ~3% of the colloids, the colloids' volume remains constant during the irradiation procedure. Figures 1(c), (d) shows a SEM side-view of silica colloids on a Si substrate of the type

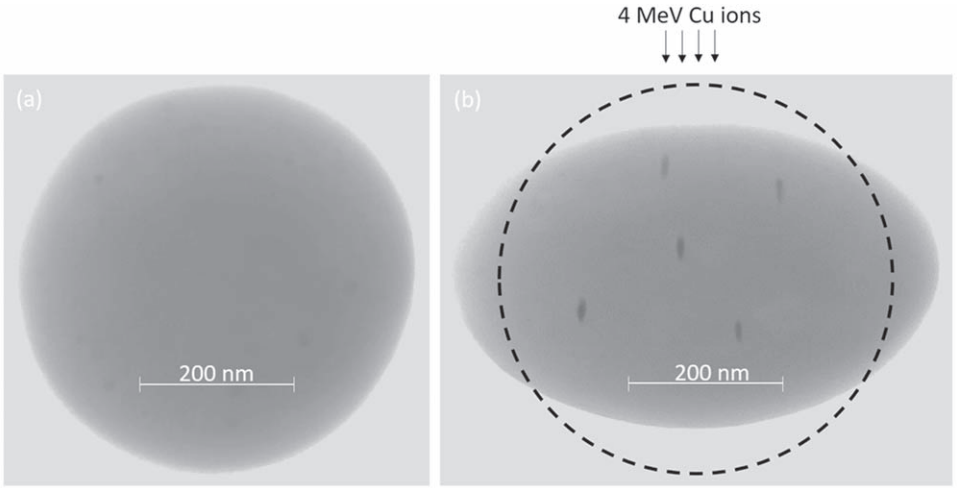

Figure 2. TEM images for colloidal Au-silica core–shell particles before and after irradiation with 4 MeV Cu ions to a fluence of 8.5×10^{14} ions cm^{-2}, (a) and (b), respectively. The direction of the ion beam is indicated by the black arrows and the circumference of the original silica colloid is indicated by the dashed circle in figure (b).

shown in figure 1(b). Figure 1(e) illustrates a SEM image of silica colloids taken in a top-down view perpendicular to the colloidal plane shown in figures 1(c), (d). It has been shown several times in the literature that the typical approach shown in figure 1(e) can be used for the fabrication of ordered two-dimensional (2D) periodic particle arrays using the nanosphere lithography (NSL) method using reference [53, 54].

As a next step, we investigated the effect of ion beam irradiation on spherical Au-silica core–shell particles with an Au core of approximately 15 nm in diameter and a silica shell of about 500 nm in diameter. In figure 2(a), we show a TEM image of an Au-silica core–shell colloid before it was irradiated. A sphere-like Au-silica colloid is evident in the image. The TEM image shown in figure 2(b) shows a surface normal image after irradiation. On the sample surface, the direction of the ion beam is indicated by the black arrows, while the radius of the original colloid is indicated by the dashed black circles. Figure 2(b) depicts the spherical silica shell expanding in the direction of the ion beam and contracting in parallel after irradiation with 4 MeV Cu ions with a maximum fluence of 8.5×10^{14} ions cm^{-2}. Calculations show that the deformed silica particle has a transverse diameter of 620 nm, increasing by 25%. As a result of the ion beam, the longitudinal diameter has decreased by about 20% (along the direction of the ion beam). The major-to-minor axis ratio (major-to-minor) at this fluence is again 1.6. By contrast, Au cores were deformed parallel to the ion beam direction. Several studies have reported elongation of the metal in the literature. Our analysis of TEM found the dimensions of the elongated Au cores to be 22 ∼23 nm × 7 ∼8 nm and the aspect ratio to be 3–4. A spherical Au core is deformed into an aligned Au nanorod under volume conservation.

We have also studied the deformation of metal particles embedded in planar SiO_2 films below an electronic loss of 2 keV nm^{-1}. Using the method described in the experimental section, we prepared colloidal Au particles in planar SiO_2 films (∼350 nm thickness). Image 3(a) depicts an AFM of a surface after colloidal Au particles are deposited. As shown in the figure, the colloidal distribution is homogeneous over the sample surface. The height profile of the deposited particles can be seen in figure 3(b) at about 15 nm (±2 nm). Measurement of the broadening of the Au peak width in the RBS spectrum gives a quick indication of the deformation of the Au colloids embedded in the SiO_2 films under ion irradiation. In figure 3(c) we show the evolution of the Au peak with fluence of 15 nm Au NPs under 4 MeV Cu ions irradiation. The inset in figure 3(c) depicts the final configuration for the irradiated Si/SiO_2-Au colloid samples. Non-irradiated samples show a sharp peak at a depth of 150 nm below the surface which corresponds to a plane of particles of 15 nm size embedded in a matrix of silica. A broadening Au RBS peak indicates that there is a greater depth range of Au as the Cu ion fluence increases. Using RBS analysis, and after normalizing the recorded data, a shift of peak energies for Au can be attributed to sputtering when irradiated at a fluence of more than 4×10^{14} ions cm^{-2}. A dashed line at channel 305 indicates the location of the Au peak. A surface channel of Au is given at channel 311. In figure 3(d), the width of the Au peak is related to the fluence of 4 MeV Cu ions. As shown in this figure, the RBS peak becomes broader at fluences above 1.8×10^{14} ions cm^{-2} and reaches saturation near 4×10^{14} ions cm^{-2}. High-resolution TEM cross-sections of the SiO_2-Au-containing layer are shown in figure 3(e). Before irradiation, the samples were prepared into a final configuration, as shown in the inset in figure 3(c). This TEM image shows the deposited Au colloids to be spherical, with a diameter of approximately 13–16 nanometers. Upon irradiation with 4 MeV Cu at a maximum fluence of 8×10^{15} ions cm^{-2}, Au colloids are significantly deformed

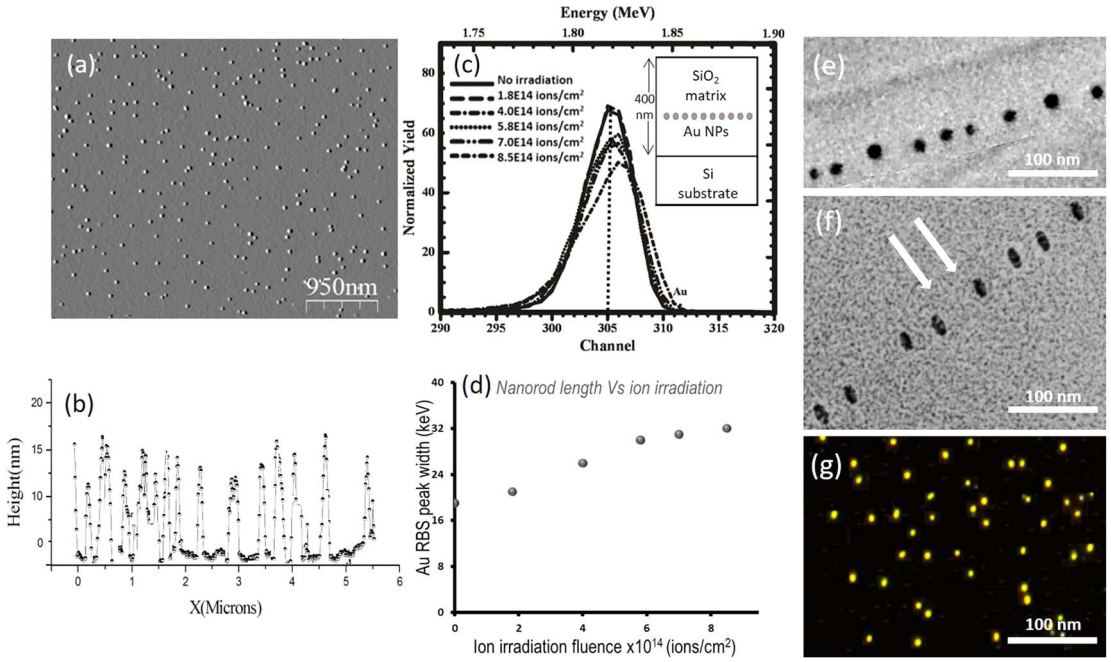

Figure 3. (a) AFM image taken from the surface of the Si/SiO_2 sample after deposition of the Au colloids. (b) The height profile of the deposited Au colloids was measured by AFM. (c) The evolution of the Au peak with fluence was obtained from RBS measurements. The inset in figure 3(c) indicates the configuration of the overall sample structure of the Si/SiO_2-Au colloids containing samples. The position of the Au peak and the surface of the Au are indicated. (d) Calculation of the Au peak width as a function of the irradiation fluence. (e) Cross-sectional X-TEM image from the unirradiated Au colloids. (f) Cross-sectional X-TEM image from the Au colloids after irradiation with 4 MeV to a fluence of 8.5×10^{14} ions cm^{-2}. (g) Dark-field optical microscope image for Au colloids after irradiation to a fluence of 8.5×10^{14} ions cm^{-2}.

(figure 3(f)). X-TEM images shown in figure 3(f) illustrate the elongated nanorods made of the original spherical Au colloids, which are about 25–28 nm long and about 6–7 nm wide with an aspect ratio of about 3 compared to the original spheres. It is estimated that the volume of these nanorods is similar to the volume of the original spherical Au colloids, i.e., $V_{\text{nanorod}} \sim V_{\text{Au colloids}}$.

A dark-field optical microscope was used to image the scattering patterns of Au colloids embedded in Si/SiO_2 films after irradiation to study the effects of ion shaping on Au colloids. In this technique, white light is shone onto the particles at a large angle (compared with the normal angle), and the scattered light is collected at a small angle. Dark-field microscopes utilize imaging mono-chromators and charge-coupled devices (CCDs) to produce true-color images of particles under a microscope. Here, the irradiation was done at a 45° angle to the surface of the sample. An image of a sample with Au particles under a Nikon dark field microscope is shown in figure 3(g) with an objective of 50x after exposure to Cu ions with a fluence of 8.5×10^{14} ions cm^{-2}. As can be seen from the image, the particles are yellow, which indicates their plasmon resonance frequency is between 620 and 650 nm. Around 90% of the particle arrays in the figure showed a color change as a result of irradiation.

We also investigated the ion-induced shaping effect on the Au colloids embedded in Si/SiO_2 films based on the nonlinear response of the metal particles, figure 4. After irradiating the Au colloids with 4 MeV Cu ions at a fluence of 8.5×10^{14} ions cm^{-2}, two peaks of the optical absorbance were observed: a peak measured at a wavelength of about 565 nm indicates the surface plasmon resonance of the colloids, and a peak measured at a wavelength of 616 nm indicates the red-shifted surface plasmon resonance. These results are consistent with the observed color of the particles in figure 3(g) and are related to the resonance of aligned anisotropic Au nanorods. Compared with spherical Au colloids, the resonance of the nanorods results in the excitation of a plasmon mode along the long axis of the nanorods.

The deformation of spherical silica colloidal or suspended metallic particles embedded in dielectrics induced by irradiation is a complex process that is affected by both the materials structure as well as the radiation itself, as first proposed by Klaumünzer [15] and later demonstrated experimentally by Penninkhof [27, 28]. Specifically, there is an anisotropic growth at high fluences and densification of around 3% at low fluences [46, 55]. Using Eshelby's theory, where the ion track is viewed as an elastic inclusion [9, 47, 48], these two mechanisms can be discussed within the concept of thermal spikes. A cylindrical region surrounding the particle track is transiently heated by electron-phonon coupling resulting from the energy of the ion introduced into the electronic subsystem. With the cooling of the thermal spike, the shear stresses become anisotropic as the ion-excited region relaxes. Silica is densified as a result of the irradiation of the surrounding area, and subsequent ion impact within

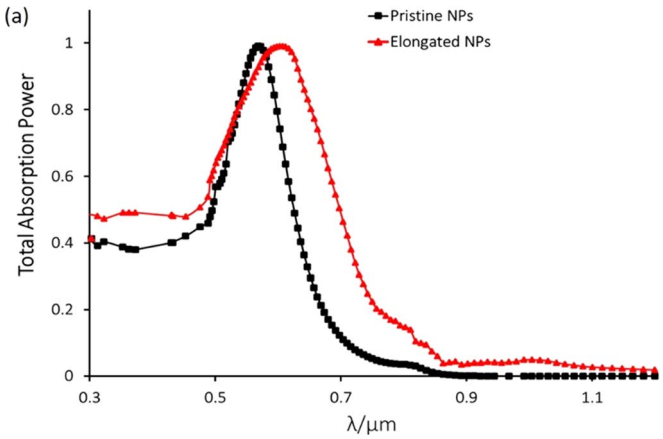

Figure 4. (a) Optical extinction spectra of Au colloids before irradiation (circles and solid black line), and under subsequent irradiation with 4 MeV Cu to a fluence of 8.5×10^{14} ions cm^{-2}, (triangles and solid red line). A red-shifted surface plasmon absorption resonances peak at a wavelength of 616 nm is observed.

the same region causes no further density change. This can be explained by the fact that the material density is irreversibly altered within every cylinder of the ion track. The deformation of the dielectric requires that impinging ions form damaged zones (called ion tracks) along their trajectories exceeding a threshold for electronic energy loss, which depends on the ion energy. In the densification phase, the anisotropic growth is negligible [55], and the metals cannot be deformed before the structural transformation of the dielectric has been completed, i.e., when the sample overlaps completely. The thermal spike nature has been proposed to interpret different crystallographic orientations of materials; see for example reference [56]. Ion irradiation of amorphous SiO_2 in various energy ranges (between 1 MeV and 1 GeV) causes structural changes [43]. It is demonstrated that high-energy ions cause the formation of track structures in silica above a threshold of electronic energy loss of 1.4 keV nm^{-1}, depending on the specific energy. Alternatively, studies on deformation thresholds of colloidal silica particles have predicted that the threshold is approximately 1 keV nm^{-1} [57, 58]. Van Dillen *et al* [59] demonstrated the anisotropic plastic deformation of spherical colloidal silica particles with a diameter of 125 nm under irradiation with Xe ions at 300 keV, e.g. 0.45 keV nm^{-1} electronic stopping at 85 K. According to Penninkhof *et al* [27, 28], systematic experiments on the colloidal Au-silica core–shell system have shown that the Au particle only deforms when the silica shell surrounding the particle exceeds a critical thickness of 30 nanometers. The experiments also show that deformation of metallic particles occurs only above a threshold of electronic energy loss in silica of about 3.3 keV nm^{-1}. However, the study by Amekura and colleagues has shown that irradiating amorphous SiO_2 with fullerene ions (C^{60+}) with high fluences of 1–6 MeV elongates metal nanoparticles in the same way as using 200 MeV Xe^{14+} heavy ions (SHI), i.e. with ions of two orders of magnitude greater energy. From these observations, it is evident that the deformation of particles is dependent on the size and amount of energy applied to the particles. Therefore, a wealth of different observations has already been published. Nonetheless, the mechanism underlying the ion-induced deformation is not yet clearly understood, at the very least, and its origin remains a subject for debate. The scientific community is not yet confident in understanding the mechanism of ion deformation, but all agree that metal particles embedded in dielectric materials, such as silica colloids and/or planar silica films, undergo ion deformation by flowing into the liquid-like tracks in the dielectric material. Therefore, elongation can only be induced at temperatures beyond those of the metal and the surrounding material [57, 58]. Nonetheless, in our current study, and in thermal spike calculations of the SiO_2/Au particle system [3, 60], it appears that neither the silica colloids and/or matrix, nor the 15 nm diameter Au particles, melt under the impact of the 4 MeV Cu ions. In contrast, we found that silica colloids with diameters of 0.5 μm and Au particles with diameters of 15 nm are deformed by 4 MeV ions. There appears to be ion-induced deformation of colloids, even in the regime in which none of the metal particles or silica is completely transiently melted [15, 29].

Conclusions

Colloidal particle-like silica, Au-silica core–shell particles, and Au-metal particles undergo anisotropic deformation when irradiated with Cu ions of about 4 MeV. In the latter case, the deformation of colloidal particles is readily detectable, without a discernible threshold for electronic energy loss in silica. Si-Au colloids and Au-silica core–shell colloids with 0.5 μm diameters exhibit anisotropic plastic deformation under 4 MeV Cu

ions, with the silica expanding perpendicular to the ion beam and contracting parallel to it, and the metal cores elongating along the beam direction. Au colloids constrained within planar SiO_2 films also exhibit elongation parallel to the ion beam. After irradiation with ions, the scattering pattern of Au colloids changes to yellow, indicating that the plasmon resonance of the particles has shifted. This was verified by optical absorption measurements, which showed a peak in the surface plasmon resonance at 616 nm. Observations of the experiments indicate that deformation occurs at an electronic energy loss in silica below 2 keV nm^{-1}. A viscoelastic model can explain the observations as a result of local shear stress relaxation in high-temperature thermal spikes caused by ions.

Acknowledgments

Not applicable.

Data availability statement

All data that support the findings of this study are included within the article (and any supplementary files).

Declarations:Ethics approval and consent to participate

No applicable.

Consent for publication

No applicable.

Availability of data and material

All data generated or analysed during this study are included in this published article.

Competing interests

The authors declare that they have no competing interests.

Funding

First and second authors acknowledge the support of Ajman University Internal Research Grant, UAE, Grant No. DSGR Ref. [2021-IRG-HBS-14].

Authors' contributions

E.A.: Coneption and design of study, acquisition of data, Formal Analysis and/or interpretation of data, funding acquisition, Writing- original draft.

E. M.: Data curation, Analysis and/or interpretation of data, Writing- original draft.

T. S.: Methodology, investigation, review editing, Writing- original draft.

ORCID iDs

E A Dawi https://orcid.org/0000-0002-1901-9807
E Mustafa https://orcid.org/0000-0002-8985-0604

References

[1] Trinkaus H and Ryazanov A I 1995 *Phys. Rev. Lett.* **74** 5072
[2] Trinkaus H 1998 *Nucl. Instrum. Methods Phys. Res. B* **146** 204
[3] Toulemonde M, Dufour C, Meftah A and Paumier E 2000 *Nucl. Instrum. Methods Phys. Res. B* **166** 903

[4] van Dillen T, Polman A, Onck P R and van der Giessen E 2005 *Physical Review. B* **71** 024103
[5] Shipway A, Katz E and Willner I 2000 *Chem. Phys. Chem* **1** 18
[6] Rogach A L, Talapin D V, Shevchenko E V, Kornowski A, Haase M and Weller H 2002 *Adv. Funct. Mater.* **12** 653
[7] Park J H, Lim Y T, Park O O, Kim J K, Yu J W and Kim Y C 2004 *Chem. Mater.* **16** 688
[8] Catchpole K R and Pillai S 2006 *J. Lumin.* **121** 315
[9] Kim S, Na S, Jo J, Kim D and Nah Y 2008 *App. Phys. Lett.* **93** 073307
[10] Haes A J, Zou S, Schatz G C and Van Duyne R P 2004 *J. Phys. Chem. B* **108** 6961
[11] Ann Bauer L, Birenbaum N S and Meyer G J 2004 *Journal of Mat. Chemistry* **14** 517
[12] D'Orléans C, Stoquert J P, Estournès C, Cerruti C, Grob J J, Guille J L, Haas F, Muller D and Richard-Plouet M 2003 *Phys. Rev. B* **67** 220101
[13] D'Orléans C, Stoquert J P, Estournès C, Grob J J, Muller D, Cerruti C and Haas F 2004 *Nucl. Instrum. Methods Phys. Res. B* **225** 154
[14] D'Orléans C, Stoquert J P, Estournès C, Grob J J, Muller D, Guille J L, Richard-Plouet M, Cerruti C and Haas F 2004 *Nucl. Instrum. Methods Phys. Res. B* **216** 372
[15] Klaumünzer S 2006 *Nucl. Instr. and Meth. in Phy. Res. B* **244** 1–7
[16] Giulian R, Kluth P, Araujo L, Sprouster D J, Byrne A, Cookson D J and Ridgway M C 2008 *Physical Review B* **78** 125413
[17] Singh F, Mohapatra S, Stoquert J P, Avasthi D K and Pivin J C 2008 Shape deformation of embedded metal nanoparticles by swift heavy ion irradiation *The Seventh Int. Symp. on Swift Heavy Ions in Matter (Lyon, France, hal-00231089)*
[18] Kluth P, Giulian R, Sprouster D J, Schnohr C S, Byrne A P, Cookson D J and Ridgway M C 2009 *Appl. Phys. Lett.* **94** 113107
[19] Kuiri P K, Joseph B, Ghatak J, Lenka H P and Sahu G 2010 *Adv. Sci. Lett.* **3** 404–10
[20] Sprouster D J, Giulian R, Araujo L L, Kluth1 P, Johannessen B, Cookson D J and Ridgway M C 2011 *J. Appl. Phys.* **109** 113504
[21] Kumar H, Ghosh S and Avasthi D K 2011 *Nanoscale Res. Lett.* **6** 155
[22] Leino A A, Pakarinen O H, Djurabekova F, Nordlund K, Kluth P and Ridgway M C 2014 *Mater. Res. Lett.* **2** 37–42
[23] Rizza G 2015 *J. Phys. Conf. Ser.* **629** 012005
[24] Amekura H, Kono K, Okubo N and Ishikawa N 2015 *Phys. Status Solidi b* **252** 165–9
[25] Peña-Rodríguez O, Prada A and Olivares J 2017 *Sci Rep.* **7** 922
[26] Roorda S, van Dillen T, Polman A, Graf C, Vredenberg A M, van Blaaderen A and Kooi B 2004 *Adv. Mater. (Weinheim, Ger.)* **16** 235
[27] Penninkhof J J, van Dillen T, Polman A, Graf C and van Blaaderen A 2005 *Adv. Mater. (Weinheim, Ger.)* **17** 1484
[28] Penninkhof J J, van Dillen T, Roorda S, Graf C, van Blaaderen A, Vredenberg A M and Polman A 2006 *Nucl. Instr. Methods Phys. Res., Sect. B* **242** 523
[29] Awazu K, Wang X, Fujimaki M, Tominaga J, Aiba H, Ohki Y and Komatsubara T 2008 *Phys. Rev. B* **78** 054102
[30] Dufour C, Khomenkov V, Rizza G and Toulemonde M 2012 *J. Phys. D* **45** 065302
[31] Giulian R, Kluth P, Araujo L L, Sprouster D J, Byrne A P, Cookson D J and Ridgway M C 2008 *Phys. Rev. B* **78** 125413
[32] Sprouster D, Giulian R, Araujo L L, Kluth P, Johannessen B, Cookson D and Ridgway M C 2011 *J. Appl. Phys.* **109** 113504
[33] Ridgway M C *et al* 2011 *Phys. Rev. Lett.* **106** 095505
[34] Benyagoub A and Toulemonde M 2015 *J. of Mat. Research* **30** 1529–43
[35] Rizza G *et al* 2012 *Phys. Rev. B* **86** 035450
[36] Coulon P-E *et al* 2016 *Sci Rep.* **6** 1
[37] Slablab A *et al* 2016 *Sci Rep.* **6** 37469
[38] Vu T H Y, Dufour C, Khomenkov V, Leino A A, Djurabekova F, Nordlund K, Coulon P-E, Rizza G and Hayoun M 2019 *NIMB* **451** 42–8
[39] Amekura H, Kluth P, Mota-Santiago P, Sahlberg I, Jantunen V, Leino A, Vazquez H, Nordlund K and Djurabekova F 2020 *NIMB* **475** 44–8
[40] Mota-Santiago P, Kremer F, Rizza G, Dufour C, Khomenkov V, Notthoff C, Hadley A and Kluth P 2020 *Phys. Rev. Materials* **4** 096002
[41] Li R *et al* 2020 *Nanotechnology* **31** 265606
[42] Lotito V and Zambelli T 2022 *Adv. Colloid Interface Sci.* **304** 102642
[43] Korkos S, Mizohata K, Kinnunen S, Sajavaara T and Arstila K 2022 *J. Appl. Phys.* **132** 04590
[44] Korkos S, Jantunen V, Arstila K, Sajavaara T, Leino A, Nordlund K and Djurabekova F 2022 *Appl. Phys. Lett.* **120** 171602
[45] Dawi E A, Rizza G, Mink M P, Vredenberg A M and Habraken F H P M 2009 *Journ. Appl. Phys.* **105** 074305
[46] Dawi E A, Rizza G, Vredenberg A M and Toulemonde M 2011 *Nanotechnology* **22** 215607
[47] Stöber W, Fink A and Bohn E 1968 *J. Coll. Interf. Sci.* **26** 62
[48] Bogush G H, Tracy M A and Zukoski C F IV 1988 *J. Non-Cryst. Solids* **104** 95
[49] Graf C, Vossen D L J, Imhof A and van Blaaderen A 2003 *Langmuir* **19** 6693
[50] Maier S A, Brongersma M L, Kik P G and Atwater H A 2002 *Phys. Rev. B* **65** 193408
[51] Tanaka Y, Obara G, Zenidaka A, Nedyalkov N N, Terakawa M and Obara M 2010 Near-field interaction of two-dimensional high-permittivity spherical particle arrays on substrate in the Mie resonance scattering domain *Opt. Exp.* **18** 27226–37
[52] Ziegler J F, Biersack J P and Ziegler M D 2013 *SRIM, a version of the TRIM program, The Stopping and Range of Ions in Matter* (http://srim.org)
[53] Hulteen J C, Treichel D A, Smith M T, Duval M L, Jensen T R and Van Duyne R P 1999 *J. Phys. Chem. B* **103** 3854–63
[54] Hulteen J C and van Duyne R P J 1995 *Vac Sci. Technol. A* **13** 1553
[55] Amekura H, Narumi K, Chiba A, Hirano Y, Yamada K, Tsuya D, Yamamoto S, Okubo N, Ishikawa N and Saitoh Y 2019 *Sci. Rep.* **9** 14980
[56] Parida B K, Sooraj K P, Hansa S, Pachchigar V, Augustine S, Remyamol T, Ajith M R and Ranjan M 2022 *Nucl. Inst and Methods B* **514** 1–7
[57] Benyagoub A, Löffler S, Rammensee M, Klaumünzer S and Saemann-Ischenko G 1992 *Nucl. Instrum. Methods Phys. Res. B* **65** 228–31
[58] van Dillen T, Polman A, Fukarek W and van Blaaderen A 2001 *Appl. Phys. Phys. Lett.* **78** 910
[59] van Dillen T, Polman A, van Kats C M and van Blaaderen A 2003 *Appl. Phys. Lett.* **83** 4315
[60] Toulemonde M, Dufour C and Paumier E 1992 *Phys. Rev. B* **46** 14362